

Energy transport and coherence properties of acoustic phonons generated by optical excitation of a quantum dot

D. Wigger,¹ S. Lüker,¹ D. E. Reiter,¹ V. M. Axt,² P. Machnikowski,³ and T. Kuhn¹

¹*Institut für Festkörperteorie, Universität Münster,
Wilhelm-Klemm-Str. 10, 48149 Münster, Germany*

²*Theoretische Physik III, Universität Bayreuth, 95440 Bayreuth, Germany*

³*Institute of Physics, Wrocław University of Technology, 50-370 Wrocław, Poland*

(Dated: April 10, 2018)

The energy transport of acoustic phonons generated by the optical excitation of a quantum dot as well as the coherence properties of these phonons are studied theoretically both for the case of a pulsed excitation and for a continuous wave (cw) excitation switched on instantaneously. For a pulsed excitation, depending on pulse area and pulse duration, a finite number of phonon wave packets is emitted, while for the case of a cw excitation a sequence of wave packets with decreasing amplitude is generated after the excitation has been switched on. We show that the energy flow associated with the generated phonons is partly related to coherent phonon oscillations and partly to incoherent phonon emission. The efficiency of the energy transfer to the phonons and the details of the energy flow depend strongly and in a non-monotonic way on the Rabi frequency exhibiting a resonance behavior. However, in the case of cw excitation it turns out that the total energy transferred to the phonons is directly linked in a monotonic way to the Rabi frequency.

PACS numbers: 63.22.-m; 63.20.kd; 43.35.Gk; 78.67.Hc

I. INTRODUCTION

The interaction between electrons and phonons plays a vital role in the optical control of semiconductor quantum dots (QDs). Besides its often decisive role for the dephasing and decoherence of electronic excitations in QDs, there has been an increasing interest in the properties of the phonons themselves, which are generated by optical excitation of the QD, and in the use of phonons for an active control of the optical properties of such nanostructures. Propagating strain waves, i.e., coherent phonon pulses, which travel through a QD or quantum well structure give rise to a dynamical shift of the optical transition frequency¹⁻⁴ which may even lead to an ultrafast switching into the lasing regime.⁵ Coherent acoustic phonons can also be used to sweep the frequency of optical cavities across the resonance frequencies of QDs.⁶ The generation of coherent phonons⁷⁻¹¹ and phonons in non-classical states such as squeezed phonons has been of considerable interest.¹²⁻¹⁵ An optically driven QD has been proposed for the realization of a phonon laser when placed in an acoustic cavity¹⁶ or it could act as a heat pump when driven non-resonantly.¹⁷ Especially in systems that reach the quantum-classical boundary the understanding of the electron-phonon coupling mechanism and the characteristic phonon properties on a microscopical level is crucial.¹⁸⁻²⁰

The impact of the electron-phonon coupling on optically induced exciton dynamics in QDs has been extensively studied in theory and experiments. Besides giving rise to a finite linewidth and a characteristic non-Lorentzian line shape of luminescence,²¹ absorption,^{22,23} or four-wave-mixing spectra,^{24,25} the coupling to phonons causes a damping of Rabi oscillations of the electronic system²⁶⁻³⁵ and it limits the achievable exciton popula-

tion inversion by chirped laser pulses via the adiabatic rapid passage.³⁶⁻⁴⁰ The efficiency of the electron-phonon coupling in the presence of a strong optical driving depends crucially and in a non-monotonic way on the laser power leading to the reappearance of Rabi rotations^{32,35} at sufficiently high pulse areas.

The main focus of the present paper is on the detailed analysis of the characteristic properties and the spatio-temporal dynamics of phonons generated by optical excitation of a QD, in particular on the degree of coherence and the energy transfer to the phonons. Furthermore we will show that studying the phonon dynamics will provide additional insight in the non-monotonic behavior of Rabi rotations as a function of the light intensity.

The QD exciton is coupled to both acoustic and optical phonons. The optical phonons, due to their in general negligible dispersion in the range of wave vectors which are coupled to the exciton, give rise to an oscillatory contribution in the optical polarization and sharp replicas in the optical spectra.^{22,23} Because of their vanishing group velocity, the optical phonons generated by this coupling remain confined to the QD region.^{14,41} As long as anharmonic processes can be neglected they do not lead to an irreversible decay of the polarization. Acoustic phonons, on the other hand, provide a continuum of states to which the QD exciton is coupled and, indeed, the coupling to acoustic phonons has been shown to be typically the main source of decoherence in optically driven QDs.^{25,35} Therefore, in this paper we will concentrate on the coupling to acoustic phonons.

For an excitation with ultrafast laser pulses, which can be approximated by δ -functions in time, the coupled exciton-phonon dynamics can be calculated analytically.^{42,43} For this case, it has been found that by the impulsive excitation a lattice deformation in the

region of the QD is created forming the acoustic polaron, which is accompanied by the emission of a phononic wave packet.^{42–46} By excitation with a tailored series of pulses the fluctuations of the phonons can be modified such that squeezed phonon wave packets can be generated.⁴³ In the case of excitation by sufficiently slowly varying light fields, on the other hand, the polaron builds up adiabatically and no phonon wave packet is emitted.⁴⁶

In this paper we will study the coupled exciton-phonon dynamics in the case of excitation by pulses with a finite pulse width as well as by a continuous light field with fixed amplitude which is instantaneously switched on. While in the absence of a light field the electron-phonon interaction in a QD is of pure-dephasing type, i.e., there are no real transitions between different electronic states, in the presence of a light field the interaction gives rise to transitions between the dressed states and therefore at sufficiently low temperatures typically to a relaxation into the lower dressed state. The two cases studied here thus represent two different aspects of non-equilibrium dynamical systems: For pulsed excitation a relaxation channel is switched on for a certain period of time and then the system returns to the pure-dephasing type. For the continuous excitation, due to the instantaneous switching on, the system is prepared in a non-equilibrium distribution over the dressed states and then it relaxes towards a new stationary state.

For both excitation conditions we will analyze quantitatively the energy transfer from the exciton to the phonon system and the energy flow associated with the emission of phonon wave packets. We will distinguish between the energy transport by coherent phonons, i.e., phonons with a non-vanishing expectation value of the displacement corresponding to a classical strain wave, and the energy flow associated with the emission of incoherent phonons, which are characterized by a vanishing mean displacement. In addition to a detailed characterization of the traveling phonon waves, the direct comparison of the time evolution of excitonic and phononic variables for varying pulse durations and light intensities will provide a common perspective on the close link between exciton dephasing and irreversibility introduced by the energy flow away from the QD by the traveling acoustic phonons and on the resonant nature of the exciton-phonon coupling in these structures. In particular we will show that although the efficiency of electron-phonon coupling is a strongly non-monotonic function of the light intensity, in the case of continuous excitation the total energy carried away by the phonons is monotonically increasing with the light intensity.

The paper is organized as follows: After the introduction, in Sec. II we summarize the theoretical background and the methods which have been used to calculate the coupled exciton-phonon dynamics. In Sec. III we begin the discussion of the results by analyzing the phonon dynamics and the corresponding energy transport resulting from a pulsed excitation of the QD. Section IV is then devoted to the coupled exciton-phonon dynamics and the

energy transport in the case of a continuous wave excitation switched on instantaneously. Finally, in Sec. V we will summarize our results and provide some concluding remarks.

II. MODEL SYSTEM

We consider a QD driven by a circularly polarized light field. The QD is taken to be in the strong confinement limit such that the electronic degrees of freedom can be reduced to a two-level system consisting of the ground state $|g\rangle$ and the single exciton state $|x\rangle$ with the angular momentum determined by the polarization of the light. The electronic system is coupled to bulk acoustic phonons via the pure dephasing mechanism, i.e., phonon-induced transitions to other electronic states are neglected because the energy separations are assumed to be much larger than the phonon energies. The Hamiltonian of the system then reads

$$\hat{H} = \hbar\omega_x|x\rangle\langle x| - \mathbf{M} \cdot \mathbf{E}^{(+)}|x\rangle\langle g| - \mathbf{M}^* \cdot \mathbf{E}^{(-)}|g\rangle\langle x| + \sum_{\mathbf{q}} \hbar\omega_{\mathbf{q}} \hat{b}_{\mathbf{q}}^\dagger \hat{b}_{\mathbf{q}} + \sum_{\mathbf{q}} \hbar \left(g_{\mathbf{q}} \hat{b}_{\mathbf{q}} + g_{\mathbf{q}}^* \hat{b}_{\mathbf{q}}^\dagger \right) |x\rangle\langle x|, \quad (1)$$

where $\hbar\omega_x$ denotes the exciton energy, $g_{\mathbf{q}}$ is the carrier-phonon coupling matrix element, $\hat{b}_{\mathbf{q}}^\dagger$ ($\hat{b}_{\mathbf{q}}$) are the creation (annihilation) operators for a phonon with wave vector \mathbf{q} and energy $\hbar\omega_{\mathbf{q}}$. $\mathbf{E}^{(\pm)}$ denotes the positive (negative) frequency component of the driving light field, which is coupled to the carriers in the usual rotating wave and dipole approximation via the dipole matrix element \mathbf{M} . We set

$$\mathbf{M} \cdot \mathbf{E}^{(+)} = \frac{\hbar}{2} \Omega(t) e^{-i\omega_L t}, \quad (2)$$

where $\Omega(t)$ denotes the instantaneous Rabi frequency and ω_L is the central frequency of the light field. In all the calculations discussed here we assume a resonant excitation, i.e., the light frequency agrees with the polaron-shifted exciton energy according to $\omega_L = \omega_x - \omega_{\text{pol}}$ with²²

$$\omega_{\text{pol}} = \sum_{\mathbf{q}} \frac{|g_{\mathbf{q}}|^2}{\omega_{\mathbf{q}}}. \quad (3)$$

For simplicity we consider a spherical QD with a harmonic confinement potential and restrict ourselves to the coupling to longitudinal acoustic (LA) phonons via the deformation potential interaction. Unless there is a strong spatial separation of electron and hole states, this is typically the dominant mechanism for phonon-induced dephasing.²⁵ A non-spherical QD shape would introduce an angular dependence in the phonon coupling and thus also in the emitted wave packet,⁴⁵ however the overall phonon emission dynamics is unchanged. We assume bulk-like LA phonons with a linear dispersion relation given by $\omega_{\mathbf{q}} = c_l q$, c_l being the longitudinal sound velocity. Due to the harmonic confinement potential, the

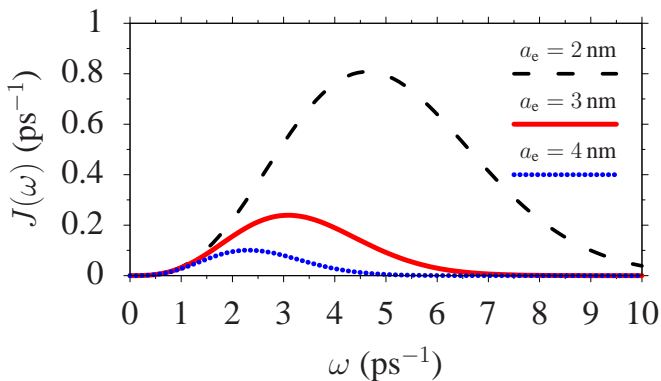


Figure 1: (Color online) Phonon spectral density $J(\omega)$ for quantum dot sizes $a_e = 2$ nm, 3 nm, and 4 nm. Calculations in this paper have been performed for $a_e = 3$ nm.

deformation potential coupling matrix element can be written in a closed form; it reads⁴²

$$g_{\mathbf{q}} = \sqrt{\frac{1}{2\rho\hbar V\omega_{\mathbf{q}}}} q \left(D_e e^{-(qa_e/2)^2} - D_h e^{-(qa_h/2)^2} \right), \quad (4)$$

where V is a normalization volume, ρ is the material density, $D_{e(h)}$ are the deformation potentials for electrons (holes), and $a_{e(h)}$ are the localization lengths of the electron (hole) wave functions. Assuming identical confinement potentials for electrons and holes, the localization lengths of electron and hole are related by the ratio of electron and hole mass according to $a_h/a_e = (m_e/m_h)^{1/4} \approx 0.87$.²²

The frequency-dependent strength of the coupling to the phonons is described by the phonon spectral density

$$J(\omega) = \sum_{\mathbf{q}} |g_{\mathbf{q}}|^2 \delta(\omega - \omega_{\mathbf{q}}), \quad (5)$$

which can directly be calculated from the coupling matrix element.^{31,44,47} Figure 1 shows this spectral density for QDs of three different sizes. The spectral density has a finite bandwidth; both the bandwidth and the maximum depend on the size expressed in terms of the electron localization a_e of the dot. For decreasing QD size, the peak position of the spectral density shifts to higher phonon frequencies and it increases in strength. In the following we will focus on a QD with an electron localization length $a_e = 3$ nm. In this case the spectral density has a maximum at approximately $\omega_{\text{ph}} = 3$ ps⁻¹, therefore the modes with this frequency couple most strongly to the exciton. The oscillation period of the most strongly coupled phonon modes is then $T_{\text{ph}} = 2\pi/\omega_{\text{ph}} \approx 2$ ps. The coupling is essentially restricted to phonons with frequencies between 1 and 6 ps⁻¹.

In this paper we are mainly interested in the energy which is transferred to the acoustic phonon system and which is carried away from the QD region by these phonons. Outside the QD region there is no energy transferred to or from the phonons leading to energy conservation in the phonon system. From elasticity theory it is

known that, similar to the case of electrodynamics, this energy conservation is reflected in an *acoustic Poynting theorem*⁴⁸

$$\frac{\partial w_{\text{LA}}(\mathbf{r}, t)}{\partial t} + \text{div}(\mathbf{S}_{\text{LA}}(\mathbf{r}, t)) = 0 \quad (6)$$

with the acoustic energy density $w_{\text{LA}}(\mathbf{r}, t)$ and the acoustic Poynting vector $\mathbf{S}_{\text{LA}}(\mathbf{r}, t)$. In our case, where only LA phonons are created, the acoustic Poynting theorem can be obtained from the wave equation for the LA phonons,

$$\frac{\partial^2 \mathbf{u}}{\partial t^2} - c_l^2 \Delta \mathbf{u} = 0, \quad (7)$$

which leads to the energy density

$$w_{\text{LA}}(\mathbf{r}, t) = \frac{\rho}{2} \left(\frac{\partial \mathbf{u}(\mathbf{r}, t)}{\partial t} \right)^2 + \frac{1}{2} \rho c_l^2 \sum_{i,j} \left(\frac{\partial u_i(\mathbf{r}, t)}{\partial x_j} \right)^2 \quad (8)$$

and the i -th component of the associated acoustic Poynting vector \mathbf{S}_{LA}

$$(S_{\text{LA}})_i = -\rho c_l^2 \sum_j \frac{\partial u_j(\mathbf{r}, t)}{\partial t} \frac{\partial u_j(\mathbf{r}, t)}{\partial x_i}. \quad (9)$$

We want to remark that Eqs. (8) and (9) differ from the general formulas obtained from elasticity theory⁴⁸ due to the restriction to an isotropic medium with only LA phonons.

In a quantum mechanical treatment, as is necessary here, the lattice displacement \mathbf{u} is replaced by the corresponding operator $\hat{\mathbf{u}}$ which, when expressed in terms of the phonon creation and annihilation operators for the LA phonons, reads

$$\hat{\mathbf{u}}(\mathbf{r}) = -i \sum_{\mathbf{q}} \sqrt{\frac{\hbar}{2\rho V\omega_{\mathbf{q}}}} \left(\hat{b}_{\mathbf{q}} e^{i\mathbf{q}\cdot\mathbf{r}} - \hat{b}_{\mathbf{q}}^\dagger e^{-i\mathbf{q}\cdot\mathbf{r}} \right) \frac{\mathbf{q}}{q}. \quad (10)$$

Accordingly, the temporal derivative $\partial \mathbf{u} / \partial t$ is replaced by $\hat{\pi} / \rho$ with the conjugate momentum operator

$$\hat{\pi}(\mathbf{r}) = - \sum_{\mathbf{q}} \sqrt{\frac{\rho\hbar\omega_{\mathbf{q}}}{2V}} \left(\hat{b}_{\mathbf{q}} e^{i\mathbf{q}\cdot\mathbf{r}} + \hat{b}_{\mathbf{q}}^\dagger e^{-i\mathbf{q}\cdot\mathbf{r}} \right) \frac{\mathbf{q}}{q}. \quad (11)$$

Then also the acoustic energy density and the acoustic Poynting vector become operators \hat{w}_{LA} and $\hat{\mathbf{S}}_{\text{LA}}$, respectively, which can be expressed in terms of the phonon creation and annihilation operators. Using the standard Bose commutation relations for these operators and integrating the energy density operator over the whole space, the free phonon Hamiltonian is recovered including the (irrelevant) zero-point energy, which has been omitted in Eq. (1), i.e.,

$$\int d^3r \hat{w}_{\text{LA}}(\mathbf{r}, t) = \sum_{\mathbf{q}} \hbar\omega_{\mathbf{q}} \left(\hat{b}_{\mathbf{q}}^\dagger \hat{b}_{\mathbf{q}} + \frac{1}{2} \right). \quad (12)$$

This confirms the consistent definition of acoustic energy density and acoustic Poynting vector for our model. In

the following, when speaking of the acoustic energy density and the acoustic Poynting vector we will refer to the expectation value of the corresponding operators, i.e.,

$$w_{\text{LA}}(\mathbf{r}, t) = \langle \hat{w}_{\text{LA}}(\mathbf{r}, t) \rangle, \quad (13a)$$

$$\mathbf{S}_{\text{LA}}(\mathbf{r}, t) = \langle \hat{\mathbf{S}}_{\text{LA}}(\mathbf{r}, t) \rangle. \quad (13b)$$

The total energy of the phonon system at time t is obtained from the phonon Hamiltonian as

$$E_{\text{LA}}(t) = \sum_{\mathbf{q}} \hbar \omega_{\mathbf{q}} \langle \hat{b}_{\mathbf{q}}^{\dagger} \hat{b}_{\mathbf{q}} \rangle. \quad (14)$$

As soon as the QD is no more in its ground state there is an additional energy contribution resulting from the exciton-phonon interaction which is given by

$$E_{\text{X-LA}}(t) = \sum_{\mathbf{q}} \hbar \left(g_{\mathbf{q}} \langle \hat{b}_{\mathbf{q}} | x \rangle \langle x | \rangle + g_{\mathbf{q}}^* \langle \hat{b}_{\mathbf{q}}^{\dagger} | x \rangle \langle x | \rangle \right). \quad (15)$$

In general, the optical excitation of the QD leads to the generation of a coherent amplitude of the lattice displacement described by the expectation value

$$\mathbf{u}(\mathbf{r}, t) = \langle \hat{\mathbf{u}}(\mathbf{r}, t) \rangle. \quad (16)$$

This coherent phonon amplitude essentially describes the dynamics of a classical strain field. In special cases, e.g., in the case of excitation by an ultrafast pulse with a pulse area given by an odd multiple of π , the phonons are generated in a purely coherent state,⁴¹ which means that

$$\langle \hat{b}_{\mathbf{q}}^2 \rangle = \langle \hat{b}_{\mathbf{q}} \rangle^2 \quad \text{and} \quad \langle (\hat{b}_{\mathbf{q}}^{\dagger})^2 \rangle = \langle \hat{b}_{\mathbf{q}}^{\dagger} \rangle^2. \quad (17)$$

In general, however, i.e., for arbitrary pulse area and pulse duration, the phonons are not generated in a purely coherent state and both coherent and incoherent phonons are emitted. Then the acoustic energy density and the acoustic Poynting vector can be separated into a coherent and an incoherent part, respectively, according to

$$(S_{\text{LA}}^{\text{coh}})_i = -\rho c_i^2 \sum_j \frac{\partial u_j(\mathbf{r}, t)}{\partial t} \frac{\partial u_j(\mathbf{r}, t)}{\partial x_i}, \quad (18a)$$

$$\mathbf{S}_{\text{LA}}^{\text{incoh}} = \mathbf{S}_{\text{LA}} - \mathbf{S}_{\text{LA}}^{\text{coh}}, \quad (18b)$$

and correspondingly for the energy density.

Because of the spherical symmetry of the system the acoustic Poynting vector has only a radial component and it depends only on the distance r from the QD center, i.e., $\mathbf{S}_{\text{LA}}(\mathbf{r}, t) = S_{\text{LA}}(r, t) \mathbf{e}_r$ with \mathbf{e}_r being the radial unit vector. Due to energy conservation, it decays $\sim r^{-2}$. To compensate for this geometrical decay, when discussing its spatio-temporal dynamics we will plot a scaled acoustic Poynting vector

$$\tilde{S}_{\text{LA}}(r, t) = \left(\frac{r}{1 \text{ nm}} \right)^2 S_{\text{LA}}(r, t), \quad (19)$$

which is defined in such a way that at a radius of 1 nm its value agrees with the true acoustic Poynting vector. By

Table I: Material parameters for GaAs

material density	ρ	5.37 g/cm ³
longitudinal sound velocity	c_l	5110 m/s
electron deformation potential	D_e	7.0 eV
hole deformation potential	D_h	-3.5 eV

integrating the acoustic Poynting vector over the surface of a sphere with radius r as well as over the past time, we obtain the total elastic energy $\mathcal{E}_{\text{LA}}(r, t)$ which has passed through that spherical surface up to time t :

$$\mathcal{E}_{\text{LA}}(r, t) = 4\pi r^2 \int_{-\infty}^t S_{\text{LA}}(r, t') dt'. \quad (20)$$

For the same symmetry reason as above and because of the restriction to LA phonons, also the displacement field associated with the coherent phonons has only a radial component and it only depends on the distance r from the QD center, i.e., $\langle \hat{\mathbf{u}}(\mathbf{r}, t) \rangle = u(r, t) \mathbf{e}_r$. Since the displacement of an emitted spherical phonon wave packet decays $\sim r^{-1}$, when showing the results in the figures below we will again compensate for this geometrical decay by plotting the scaled quantity

$$\tilde{u}(r, t) = \left(\frac{r}{1 \text{ nm}} \right) u(r, t). \quad (21)$$

The coherent part of the acoustic energy density and the acoustic Poynting vector can be directly expressed in terms of the radial displacement according to

$$w_{\text{LA}}^{\text{coh}}(r, t) = \frac{1}{2} \rho \left[\left(\frac{\partial u}{\partial t} \right)^2 + c_l^2 \left(\frac{\partial u}{\partial r} \right)^2 \right] \quad (22a)$$

$$S_{\text{LA}}^{\text{coh}}(r, t) = -\rho c_l^2 \frac{\partial u}{\partial t} \frac{\partial u}{\partial r}. \quad (22b)$$

While in the case of excitation by ultrafast laser pulses the coupled QD-phonon dynamics can be calculated analytically,⁴² for pulses with finite duration and for cw excitation no exact analytical results are known. Therefore we use a numerical calculation on the level of a fourth-order correlation expansion^{49,50} which has been shown to provide very reliable results in the parameter range studied here.⁵¹ From the calculations we obtain the coherent phonon mode amplitudes $\langle \hat{b}_{\mathbf{q}} \rangle$ and $\langle \hat{b}_{\mathbf{q}}^{\dagger} \rangle$ which, according to Eq. (10), determine the displacement field $\langle \hat{\mathbf{u}}(\mathbf{r}, t) \rangle$ and thus all other coherent phonon-related quantities introduced above. In addition we get the expectation values of products of phonon operators $\langle \hat{b}_{\mathbf{q}} \hat{b}_{\mathbf{q}'} \rangle$, $\langle \hat{b}_{\mathbf{q}}^{\dagger} \hat{b}_{\mathbf{q}'} \rangle$ and $\langle \hat{b}_{\mathbf{q}}^{\dagger} \hat{b}_{\mathbf{q}'}^{\dagger} \rangle$, from which the total acoustic energy and the total acoustic Poynting vector can be calculated. Since we are interested in excitation induced properties of the phonons, we restrict ourselves to the temperature $T = 0$ K. Initially both the exciton and the phonon system are taken to be in their respective ground state. The material parameters taken in the calculations are summarized in Table I.

III. PULSED EXCITATION

Let us first consider the case of excitation by a Gaussian laser pulse with pulse area A and pulse width τ , where the Rabi frequency entering in Eq. (2) is given by

$$\Omega(t) = \frac{A}{\tau\sqrt{2\pi}} \exp\left(-\frac{t^2}{2\tau^2}\right). \quad (23)$$

In an ideal two-level system without coupling to phonons, the excitation by a pulse with pulse area $A = \pi$ completely inverts the system. In the present case, due to the exciton-phonon coupling, the excitation of the electronic system is in general associated with an excitation of the phonon system resulting in a dephasing of the electronic system and the generation of coherent and incoherent phonons.⁵⁰ Both the dephasing and the phonon generation have been found to strongly depend on the pulse width τ .^{31,46,50} In the following we will review the acoustic phonon dynamics and in particular analyze the energy transfer to and energy transport by the acoustic phonons in the case of excitation by pulses with different pulse areas and pulse widths.

Figure 2 shows for the case of excitation by a π -pulse with width $\tau = 100$ fs [Fig. 2(a)] and $\tau = 5$ ps [Fig. 2(c)] the occupation of the exciton state $f = \langle |x\rangle\langle x| \rangle$ as a function of time (lower panels) and the coherent lattice displacement $\tilde{u}(r, t)$ as a function of time and distance from the QD (upper panels). (Note that the plotted displacement has been scaled according to Eq. (21).) While the exciton occupation in both cases essentially reaches one, the resulting phonon dynamics is very different. In both cases a negative lattice displacement builds up in the region of the QD, i.e., the lattice contracts radially towards the QD (horizontal blue lines at $r \lesssim 5$ nm). In addition, in Fig. 2(a) a pronounced negative displacement outside the QD region shows up (diagonal blue line) while in Fig. 2(c) essentially no displacement outside the QD region is seen.

The lattice displacement in the QD region results from the fact that, according to the linear exciton-phonon coupling in Eq. (1), the equilibrium positions of the lattice ions are shifted if the electronic system is in its excited state. The horizontal lines therefore depict the build-up of the acoustic polaron in the QD region.

As has been discussed in previous studies,⁴⁶ the two pulse durations shown in Fig. 2 correspond to two limiting cases: In the case of the long pulse with $\tau = 5$ ps [Fig. 2(c)], the temporal evolution occurs on a time scale slower than the characteristic time scale of the phonons, which can be estimated as the oscillation period of the most strongly coupled phonon mode, $T_{\text{ph}} \approx 2$ ps. In this case the lattice ions move adiabatically into their new equilibrium positions. In contrast, in the case of the short pulse [Fig. 2(a)] the excitation of the electronic system occurs much faster than T_{ph} , such that the phonons cannot follow immediately. Instead, the polaron builds up after the pulse and the excess energy which is released by the polaron formation is emitted in the form of a phonon

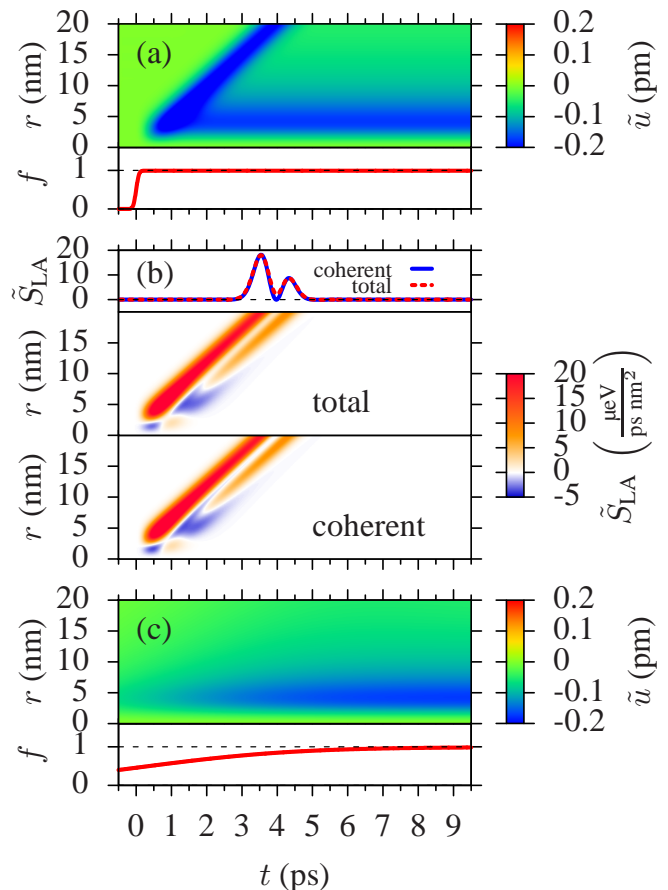


Figure 2: (Color online) (a) Coherent lattice displacement $\tilde{u}(r, t)$ [scaled according to Eq. (21)] as a function of time t and distance from the QD center r (upper panel) and occupation f of the exciton state as a function of time (lower panel) for the case of excitation by a laser pulse with pulse area $A = \pi$ and pulse width $\tau = 100$ fs. (b) Total and coherent acoustic Poynting vector of the LA phonons $\tilde{S}_{\text{LA}}(r, t)$ [scaled according to Eq. (19)] as functions of time t and distance from the QD center r (lower and central panel) and as a function of time at $r = 20$ nm (upper panel). (c) Same as part (a) but for a π -pulse with pulse width $\tau = 5$ ps.

wave packet which leaves the QD region with the sound velocity c_l [diagonal blue line in Fig. 2(a)]. The emitted wave packet has a temporal width of about 1 ps which is directly related to the bandwidth of the phonon spectral density.

In Fig. 2(b) we have plotted the acoustic Poynting vector of the LA phonons \tilde{S}_{LA} [scaled according to Eq. (19)] for the case of excitation by the 100 fs pulse. The lower and central parts show the coherent and total acoustic Poynting vector, respectively, as functions of time and distance from the QD, the upper part shows both quantities as functions of time at the distance of $r = 20$ nm. We observe that the coherent and the total acoustic Poynting vector exhibit an almost perfect agreement indicating that in this case the phonons are generated in an almost perfect coherent state. Since the Poynting vec-

tor associated with coherent phonons is determined by the temporal and spatial derivatives of the displacement [see Eq. (18a)], the emitted phonon wave packet gives rise to a double-peak structure with maxima at the rising and falling edge of the wave packet and a minimum in the center. Only at this minimum a slight difference between coherent and total Poynting vector is seen. In the case of excitation by the 5 ps pulse no phonon wave packet is emitted and thus the acoustic Poynting vector is very small and therefore it is not shown.

The spatio-temporal evolution of the lattice displacement in the case of the short pulse excitation agrees well with calculations in the δ -pulse limit discussed in Ref. 43, where the exciton and phonon dynamics can be calculated analytically without any approximation.⁴² In particular, it can be shown that the excitation by an ultrafast π -pulse indeed results in the generation of purely coherent phonons.¹⁴ From the excellent agreement we can conclude that, on the one hand, the δ -pulse limit is in this system a reasonable approximation for laser pulses with durations in the range of hundred femtoseconds, and that, on the other hand, the fourth-order correlation expansion is an adequate approximation to describe the phonon dynamics with high precision.

When the pulse area of the exciting laser pulse is increased to $A = 2\pi$, the electronic system is first excited and subsequently de-excited again. In an ideal two-level system the exciton occupation thus returns to zero after the pulse. Figure 3 shows the exciton and phonon dynamics of the coupled exciton-phonon system for the case of excitation by a 2π -pulse with pulse widths (a) $\tau = 0.5$ ps and (c) $\tau = 5$ ps.

In the case of the long pulse [Fig. 3(c)] we observe again the quasi-adiabatic evolution of the exciton-phonon system. With increasing occupation of the exciton the polaron builds up and with the subsequent decrease in the occupation also the polaron decays such that after the pulse no excitation is left, neither in the electronic nor in the phonon system. The other limiting case of excitation by an ultrafast pulse with $\tau \lesssim 100$ fs is not shown here, because in this case the electronic system is so rapidly excited and de-excited that the phonon system cannot follow and essentially remains in its ground state. For an intermediate pulse width of $\tau = 0.5$ ps [Fig. 3(a)] we find that the rapidly rising exciton occupation is associated with the build-up of a polaron and the emission of a phonon wave packet with a negative displacement (blue diagonal line). The subsequent decrease of the occupation leads to a decay of the polaron which, because of the rather short time scale, is again associated with the emission of a phonon wave packet, now however with a positive value of the displacement (yellow-red diagonal line). The irreversibility introduced by the emission of the phonon wave packet gives rise to the dephasing of the electronic degrees of freedom. As a result, the exciton occupation does not completely return to zero.

When looking again at the acoustic Poynting vector [Fig. 3(b)], we now observe a pronounced difference be-

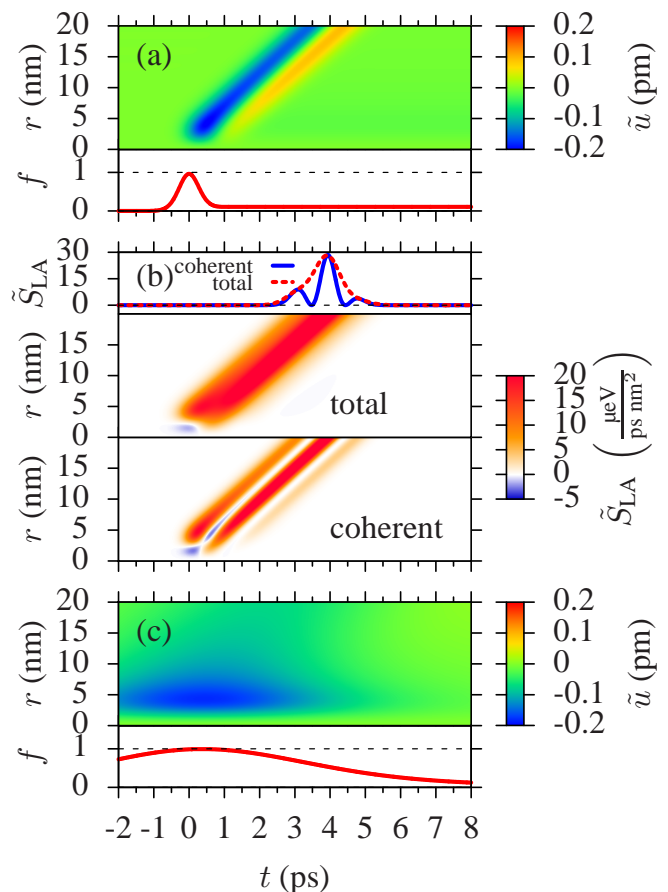


Figure 3: (Color online) Same as Fig. 2 but for a pulse area of $A = 2\pi$ and pulse widths $\tau = 0.5$ ps [parts (a) and (b)] and $\tau = 5$ ps [part (c)].

tween the total energy flow and the energy flow associated with coherent phonons. The coherent acoustic Poynting vector exhibits three peaks located at the positions of maximal slopes of the displacement profile. The total Poynting vector instead is a smooth function of time which forms an envelope over the coherent part showing that between the peaks resulting from the coherent phonons there is still an energy transport but now related to incoherent phonons.

The energy dissipation to the phonon system after excitation by pulses with different pulse areas is summarized in Fig. 4(a), where we have plotted the total elastic energy $\mathcal{E}_{\text{LA}}(r = 20 \text{ nm}, t = \infty)$, which flows through the surface of a sphere with 20 nm radius after excitation by a pulse with pulse area $A = n\pi$ as a function of the pulse width τ for $n = 1, \dots, 6$. The radius $r = 20$ nm has been chosen such that the polaron contribution to the energy flow is negligible. Outside of the polaron region the total energy $\mathcal{E}_{\text{LA}}(r, t = \infty)$ flown through the surface of a sphere with radius r is in fact independent of r .

Let us first concentrate on the two curves corresponding to pulse areas π and 2π . While in the limit of long pulses for both pulse areas the adiabatic limit is reached,

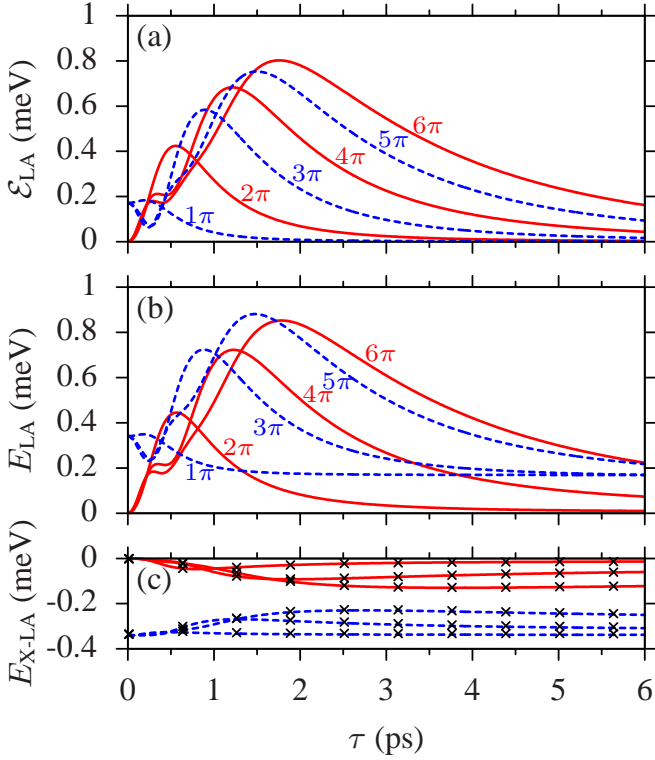


Figure 4: (Color online) (a) Total energy carried away by the phonons, (b) total energy transferred to the phonon system, and (c) final exciton-phonon interaction energy as a function of the pulse width τ of the exciting laser pulse for pulses with pulse areas $A = n\pi$ for $n = 1, \dots, 6$. For the blue dashed curves in (c) (pulse areas of odd multiples of π) the pulse area increases from bottom to top; for the red solid lines (pulse areas of even multiples of π) the pulse area increases from top to bottom. The symbols in (c) show the energy $-2f\hbar\omega_{\text{pol}}$ with the calculated exciton occupation f at the respective pulse width and pulse area.

in which the phonon dynamics is restricted to the QD region and no energy is emitted, for short pulses there are pronounced differences. In the case of excitation by a π -pulse the emitted energy becomes maximal in the limit of ultrafast pulses and decays monotonically with increasing pulse width. In contrast, for a 2π -pulse the dynamics of the exciton is decoupled from the phonon dynamics in the limit of ultrafast pulses. Hence, there is no energy emitted. Here, the emitted acoustic energy becomes maximal for pulse widths of about 0.5 ps.

When increasing the pulse area A beyond 2π , the electronic system performs multiple Rabi rotations. The characteristic time scale of the electronic evolution increasingly deviates from the pulse width τ . Instead it is determined by the instantaneous Rabi period $2\pi/\Omega(t)$ which then determines the coupling to the phonons. In Fig. 5 the exciton and phonon dynamics are shown for the case of excitation by pulses with a pulse area of $A = 6\pi$ and a pulse width of $\tau = 0.5$ ps [Figs. 5(a) and (b)] and $\tau = 2$ ps [Figs. 5(c) and (d)]. The exciton occupation per-

forms three Rabi flops and, in the case of the short pulse, essentially returns to zero while for the longer pulse an occupation of about 0.3 remains which already indicates a rather strong dephasing. In the case of the short pulse [Fig. 5(a)] we observe the emission of a wave packet with negative amplitude resulting from the initial increase of the occupation and a wave packet with positive amplitude caused by the de-excitation during the trailing edge of the pulse. The Rabi oscillations in between occur on a shorter time scale of the order of 100 fs, which is faster than the typical phonon time scale, and therefore they are almost decoupled from the phonons. In contrast, for the longer pulse [Fig. 5(c)] the period of the Rabi oscillations is in the range where the exciton-phonon coupling is rather efficient. We observe the emission of three pronounced wave packets with a negative amplitude associated with a rising exciton occupation and in between two wave packets with positive amplitude associated with the decreasing occupation. The final decay is rather weak due to the strong dephasing and therefore does not anymore lead to a clear coherent phonon emission.

Figures 5(b) and (d) illustrate the energy flow associated with the generated phonons for the two pulse durations. In the case of the longer pulse, the total acoustic Poynting vector again forms an envelope over the peaks associated with the emission of coherent phonons. For the shorter pulse, on the other hand, the total energy flow goes to zero at the center of the wave packet. Here the decoupling between exciton and phonons due to the fast exciton dynamics also inhibits the generation of incoherent phonons. The total acoustic Poynting vector now exhibits a double peak structure.

Let us now come back to the discussion of the emitted energy. In addition to the cases of $A = \pi$ and $A = 2\pi$, Fig. 4(a) shows the total energy transported away from the QD by the phonon wave packets also for pulses with higher pulse areas. For even multiples of π all curves start at zero while for odd multiples all curves start at the same finite value. This is due to the fact that for very short pulses the exciton dynamics is decoupled from the phonons and the subsequent phonon dynamics only depends on the final exciton occupation, which is zero for even multiples and one for odd multiples of π . The maxima of the curves increase with increasing pulse area and they shift to higher values of the pulse width. This shift again reflects the fact that the efficiency of the coupling is determined by the Rabi frequency instead of the pulse width. As can be seen from Eq. (23), a larger pulse area A requires a larger pulse width τ to reach the same peak Rabi frequency $\Omega_{\text{max}} = (A/\tau\sqrt{2\pi})$. The increase in the emitted energy at the maximum of the curve with increasing pulse area is due to the fact that each Rabi flop gives rise to the emission of a pair of wave packets. Since, however, as seen in Fig. 5(b), the amplitude of subsequent Rabi flops decreases due to an increasing dephasing, the maximally emitted energy does not grow linearly with the pulse area but in a sub-linear way.

Interestingly, all curves for $A \geq 3\pi$ exhibit a local mini-

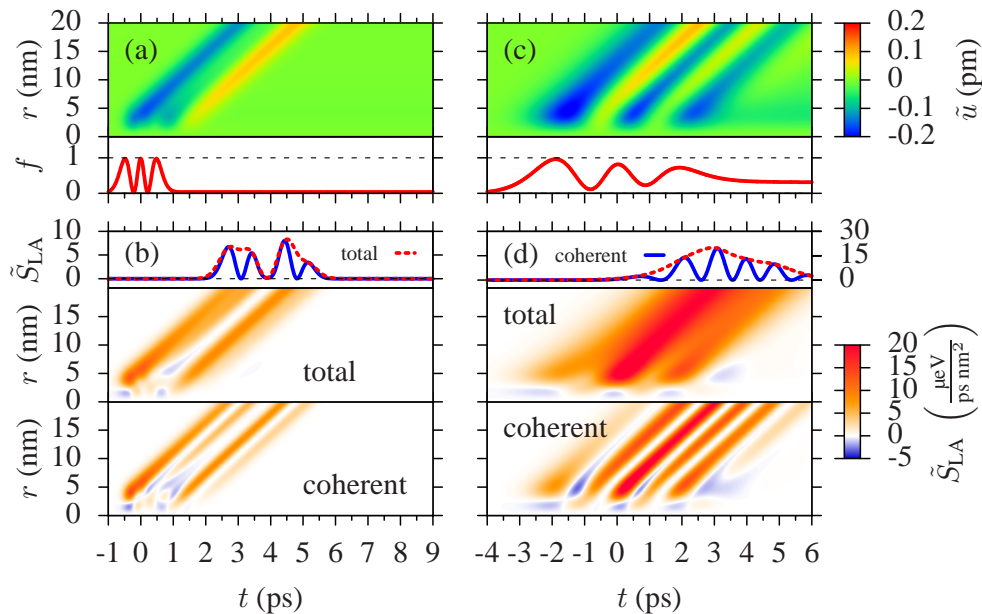


Figure 5: (Color online) Same as Fig. 2 but for a pulse area of $A = 6\pi$ and pulse widths $\tau = 0.5$ ps [parts (a) and (b)] and $\tau = 2$ ps [parts (c) and (d)].

mum at short pulse widths before reaching their maximal value. This minimum results from the fact that at these short pulses there is a significant destructive interference between wave packets with negative amplitude emitted during the rise of the excitonic occupation and those with positive amplitude emitted during the decrease of the occupation. This destructive interference reduces the energy transported away from the QD by the phonon wave packets. In particular in the case of pulses with pulse areas given by odd multiples of π this leads to a rapid initial decrease of the emitted phonon energy for very short pulses.

Figure 4(b) shows the total energy of the phonon system $E_{\text{LA}}(t = \infty)$ calculated according to Eq. (14). For pulse areas given by even multiples of π the curves in Fig. 4(b) are very similar to the ones in Fig. 4(a). In these cases there is only a small exciton occupation after the pulse and thus there is only a small polaron contribution remaining. Therefore, almost all of the energy transferred to the phonons is transported away from the QD region. In the case of pulse areas given by odd multiples of π the QD essentially remains in the excited state after the pulse which is associated with a polaronic lattice distortion in the QD region. The total energy of the phonons is therefore larger than the energy transported away, the difference being given by the energy of the polaron.

This interpretation is confirmed and quantified by looking at the interaction energy calculated according to Eq. (15), which is plotted in Fig. 4(c). In the ultrafast limit the interaction energy is $-2\hbar\omega_{\text{pol}}$ for all odd multiples of π while it vanishes for all even multiples. This is because in the former case the exciton occupation after

the pulse is given by $f = 1$ while in the latter case it is $f = 0$. For larger pulses, due to the dephasing during the pulse, there is a non-zero final occupation after pulses with an integer multiple of π and a non-unit occupation after pulses with an odd multiple of π . Thus the interaction energy is in general between the limiting cases found for ultrafast pulses. For long pulses we approach the adiabatic regime where again these values are reached. This is seen in particular in the cases of π and 2π pulses while for pulses with higher pulse areas much longer pulse widths are required to reach this regime. We find that the interaction energy in all cases is given by $-2f\hbar\omega_{\text{pol}}$ [symbols in Fig. 4(c)]. Furthermore, the energies shown in Fig. 4 satisfy the relation

$$E_{\text{LA}} - \mathcal{E}_{\text{LA}} = -\frac{1}{2}E_{\text{X-LA}}, \quad (24)$$

confirming again that indeed except for the energy residing in the polaron all the remaining energy is emitted from the QD.

From the results discussed so far we can conclude that the instantaneous Rabi frequency has a significant impact on the phonon emission of the QD. On the one hand, very slow excitations adiabatically build up and remove the polaron and, on the other hand, very fast Rabi oscillations lead to a decoupling of exciton and phonon dynamics. Only for intermediate Rabi frequencies we find an efficient carrier-phonon coupling leading to a pronounced transfer of energy to the phonons and a subsequent transport of energy away from the QD region. To analyze this resonance phenomenon in more detail, in the next section we will study the case of excitations in which the Rabi frequency is fixed after the optical field has been switched on.

IV. CONTINUOUS EXCITATION SWITCHED ON INSTANTANEOUSLY

In this section we consider a light field that is switched on instantaneously at $t = 0$. After the switching-on the amplitude of the light field remains constant, so that the Rabi frequency in Eq. (2) is time-independent, i.e., $\Omega(t) = \Omega_R$. The associated Rabi period is $T_R = 2\pi/\Omega_R$. A continuously driven two-level system which is coupled to phonons performs damped Rabi oscillations. In the limit of long times the system reaches a stationary state, where in the case of resonant driving the occupation of the exciton is $f = 0.5$ and the polarization depends on the coupling to the phonons.⁵¹ Here we again want to focus on the properties of the generated phonons.

First we analyze the case when the Rabi frequency is equal to the frequency where the phonon spectral density has its maximum, i.e., $\Omega_R = \omega_{\text{ph}} = 3 \text{ ps}^{-1}$. Figure 6(a) shows in the lower panel the occupation of the exciton state f as a function of time after switching on the light field. One clearly observes Rabi oscillations with a period of $T_R \approx 2 \text{ ps}$ that are strongly damped in time. Already after 20 ps a stationary occupation of $f = 0.5$ is reached. In the lattice displacement \tilde{u} shown in the central panel a series of diagonal lines with alternating sign appears reflecting emitted phonon wave packets. The amplitudes are getting smaller with every line. For long times the lines almost vanish and only a weak horizontal line around $r \approx 5 \text{ nm}$ remains. This line represents the polaron which is reduced compared to Fig. 2 due to the reduced exciton occupation of $f = 0.5$ in the stationary state. For every Rabi flop a pair of wave packets, one with negative and one with positive amplitude, is emitted. While the first wave packets have large amplitudes, the amplitudes get smaller quite fast. All the features of the wave packets can also be seen in the upper panel where we show \tilde{u} as a function of time for the fixed distance of $r = 20 \text{ nm}$. We notice that the first wave packet arrives at $t = 4 \text{ ps}$, which is the time the phonons need to cover a distance of 20 nm. Both, in the oscillation period and the damping behavior we see a strong analogy between the lattice displacement and the Rabi oscillation, reflecting the tight connection between the two systems. The small lattice displacement remaining for long times is the tail resulting from the polaronic displacement, which is still slightly visible even at a distance of $r = 20 \text{ nm}$. It agrees with the value of the polaronic displacement at this distance calculated analytically for the case of ultrafast excitation⁴³ included as dashed line in the plot, which demonstrates that the lattice distortion associated with the polaron is an intrinsic feature of the system and independent of the details of excitation.

Figure 6(b) shows the acoustic Poynting vector \tilde{S}_{LA} scaled according to Eq. (19). The lower panel displays the coherent part and the central panel the total value, both plotted as functions of time and distance from the QD. The upper panel shows the coherent as well as the total value at a distance of 20 nm from the QD as a

function of time. Like in the case of pulsed excitation we find peaks in the coherent part of the energy at the edges of the coherent phonon wave packets while the total acoustic Poynting vector is a smooth function of time and forms an envelope over the coherent part. Both the coherent and incoherent phonon emission are strongly damped on the same time scale as the oscillations in the exciton occupation. While in the region far from the QD the energy flow is always positive, i.e., directed away from the QD, close to the QD at distances $r \lesssim 5 \text{ nm}$ an oscillation of the acoustic Poynting vector between negative and positive values appears. This pattern shows the effect of the creation and destruction process of the polaron in the QD area. The steady contraction and relaxation of the lattice atoms leads to an oscillatory behavior of the energy in an area close to the QD which is obviously not only associated with the oscillatory energy transfer between exciton and phonons but also with a spatial flow of energy in the phonon system to and from the QD region.

Let us now consider the case of a Rabi frequency twice as large as previously studied, i.e., $\Omega_R = 6 \text{ ps}^{-1}$. Figure 6(c) shows in the lower panel the corresponding Rabi oscillation, which has an oscillation period of 1 ps. We can see that now the oscillation is only slightly damped. The lattice displacement in the central and upper panels shows a sequence of phonon wave packets emitted with the same frequency as the Rabi oscillations. Compared to the first wave packet the remaining wave packets of this sequence have only small amplitudes. The first wave packet is emitted at $t = 0$ and has a width of approximately 1 ps. It is a result of the instantaneous switching-on of the light field. During the rest of the time only weak wave packets are emitted. This is a result of the high driving frequency of the exciton system, which is too fast for the lattice atoms to follow.

Looking now at the acoustic Poynting vector in Fig. 6(d), a constant series of diagonal lines with significant amplitudes is visible both in the coherent part and the total energy flow. Although the emitted wave packets are quite weak, they carry a remarkable amount of energy with them. In addition, the amplitudes are almost undamped on the time scale shown here. In the region close to the QD we again see the oscillatory behavior of the energy flux.

Finally we take $\Omega_R = 1.5 \text{ ps}^{-1}$, i.e., half the value of Figs. 6(a),(b). The results are shown in the right column of Fig. 6. The Rabi oscillation in the occupation plotted in the lower panel of Fig. 6(e) has an oscillation period time of about 4 ps and only a moderate damping. The lattice displacement in the central and upper panel shows again a sequence of wave packets emitted from the dot. The wave packets are clearly visible over the whole time window and have the same damping as the Rabi oscillation. The acoustic Poynting vector in Fig. 6(f) has the same features as in the two cases discussed before, but in comparison to the amplitude of the lattice displacement in Fig. 6(a) it is rather weak. This shows that, because of the much lower temporal derivative of the displacement,

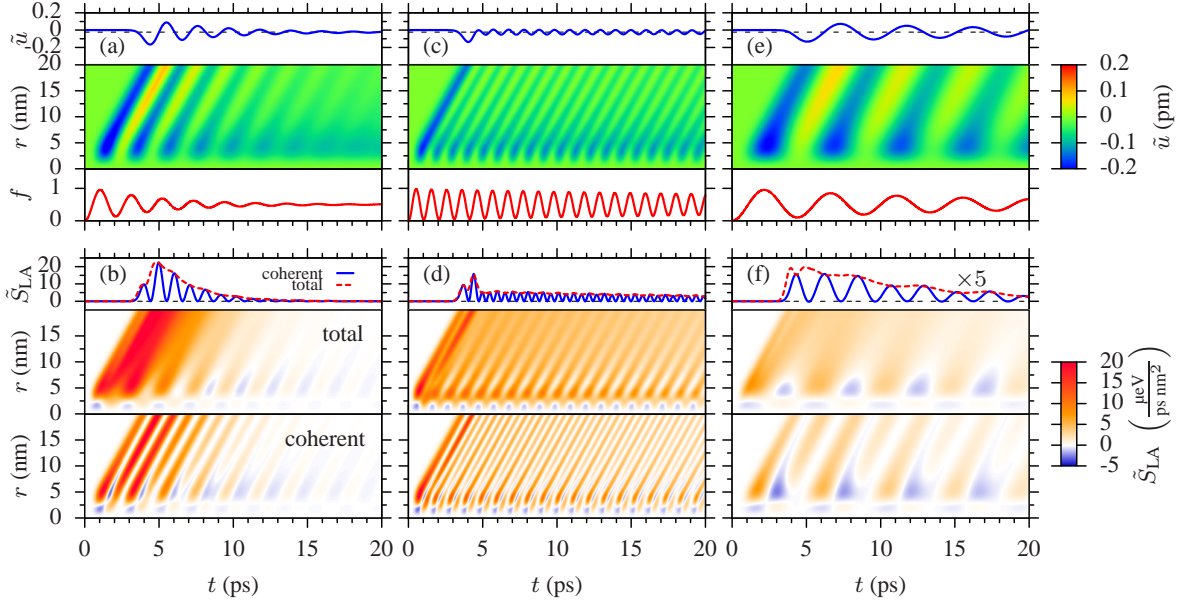


Figure 6: (Color online) (a),(c),(e) Coherent lattice displacement $\tilde{u}(r, t)$ [scaled according to Eq. (21)] as a function of time t and distance r from the QD center r (central panels) and as a function of time at $r = 20 \text{ nm}$ (upper panels) and occupation f of the exciton state as a function of time (lower panels) for a cw excitation switched on at time $t = 0$. (b),(d),(f) Total and coherent acoustic Poynting vector of the LA phonons $\tilde{S}_{LA}(r, t)$ [scaled according to Eq. (19)] as functions of time t and distance from the QD center r (central and lower panels) and as a function of time at $r = 20 \text{ nm}$ (upper panels). The Rabi frequencies are (a),(b) $\Omega_R = 3 \text{ ps}^{-1}$; (c),(d) $\Omega_R = 6 \text{ ps}^{-1}$; (e),(f) $\Omega_R = 1.5 \text{ ps}^{-1}$.

these broad wave packets carry only a small amount of energy.

After discussing these three examples of excitation with a Rabi frequency at, above, and below the phonon resonance frequency, let us now summarize these findings by discussing the dependence of the phonon emission properties on the Rabi frequency. For this purpose, in Fig. 7 characteristic variables of the exciton and phonon system are plotted as functions of time t and Rabi frequency Ω_R . Figure 7 (a) shows the exciton occupation f . As expected, the electronic system performs damped oscillations between the ground state and the exciton state with Rabi frequency Ω_R , the damping being strongly dependent on the Rabi frequency. The dashed line marks the resonance frequency $\Omega_R = 3 \text{ ps}^{-1}$, where the spectral density has its maximum. Indeed, at this Rabi frequency the dephasing is most efficient. In a region around this resonant Rabi frequency the oscillations vanish very fast. For long times the occupation f reaches a stationary value of 0.5. For frequencies outside this region the Rabi oscillations are rather stable on the time scale considered here.

To analyze the properties of the emitted phonon wave packets we focus on a fixed distance of $r = 20 \text{ nm}$. At this distance the influence of the polaron is negligible, so that the effects of the emitted wave packets can clearly be seen. Figure 7(b) shows the lattice displacement, where the dashed line again marks $\Omega_R = 3 \text{ ps}^{-1}$. The first wave packet shows up at $t \approx 4 \text{ ps}$, which is attributed to the time that the phonons need to cover a distance of 20 nm

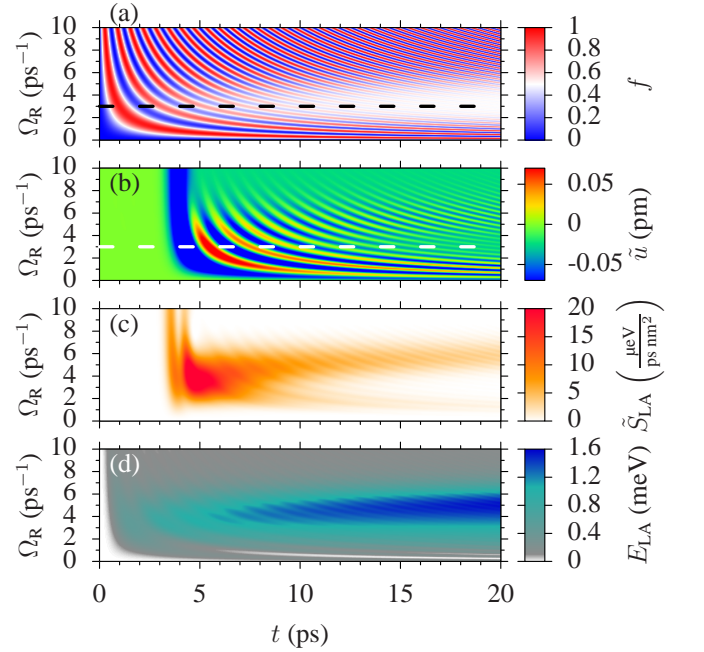


Figure 7: (Color online) Exciton and phonon dynamics as a function of time t and Rabi frequency Ω_R for a cw excitation switched on at time $t = 0$. (a) Exciton occupation f , (b) scaled lattice displacement \tilde{u} at a distance of $r = 20 \text{ nm}$, (c) scaled total acoustic Poynting vector \tilde{S}_{LA} at $r = 20 \text{ nm}$, and (d) total energy of the phonon system E_{LA} .

after they have been created at $t = 0$. This wave packet is very pronounced and appears as soon as the Rabi frequency is sufficiently high. Furthermore, the shape of this wave packet is almost independent of Ω_R . As seen in Fig. 6, this wave packet is a fingerprint of the instantaneous switching-on of the light field and therefore not sensitive to the Rabi frequency itself.

In agreement with the behavior of the Rabi oscillations, the amplitudes of the emitted phonon wave packets are strongly damped around the resonance frequency $\Omega_R = 3 \text{ ps}^{-1}$ showing a coincidence in the damping behavior between carriers and phonons. For frequencies smaller than 3 ps^{-1} the exciton creation and destruction is slower than the phonon dynamics, so that the emission of broad wave packets is possible [cf. Fig. 6(f)]. An efficient phonon emission is also possible when the Rabi frequency exceeds the resonance frequency, but in this case the repetition rate of the wave packets is much higher than in the low frequency limit. If the Rabi frequency is increased even more, i.e., for $\Omega_R \gtrsim 8 \text{ ps}^{-1}$, the phonons become essentially decoupled from the carrier dynamics. This is confirmed by the vanishing amplitudes of the lattice displacement after the pronounced wave packet emitted at $t = 0$. For the exciton occupation this decoupling leads to almost undamped Rabi oscillations, leading to the reappearance of Rabi rotations when plotted as a function of the pulse area.³²

To analyze the energy transport associated with the generated phonons, in Fig. 7(c) the scaled total acoustic Poynting vector \hat{S}_{LA} at the distance $r = 20 \text{ nm}$ is shown. The acoustic Poynting vector also shows a pronounced damping behavior in the resonance region around 3 ps^{-1} , where the energy flow decays within a few picoseconds after the first wave packet arrives. In contrast, the energy emission lasts much longer if the Rabi frequency is slightly increased above the phonon resonance. Especially for Rabi frequencies around $\Omega_R = 5 \text{ ps}^{-1}$ we observe a significant and stable energy flux for the times shown here. Moving to smaller values of $\Omega_R \approx 1 \text{ ps}^{-1}$, the energy flux also lasts quite long. But despite the pronounced lattice displacements occurring at these Rabi frequencies, the wave packets carry only little energy because of the small velocities of the displacement associated with the low frequencies. This can be seen in the comparably small values of the acoustic Poynting vector.

Another illustrative quantity to characterize the phonon emission efficiency is the total energy $E_{LA}(t)$ transferred to the phonons up to the time t , which is shown in Fig. 7(d). While the phonon energy reaches its final value within the shortest time at the resonance frequency $\Omega_R = 3 \text{ ps}^{-1}$, the overall maximal energy emission within the time span of 20 ps shown here is found around $\Omega_R = 5 \text{ ps}^{-1}$. For resonant coupling the energy transfer is strongest for short times, but vanishes quickly as the exciton system reaches its stationary state. Instead, for higher Rabi frequencies the phonon emission is present for a longer time. Although each wave packet carries a smaller amount of energy than at resonance,

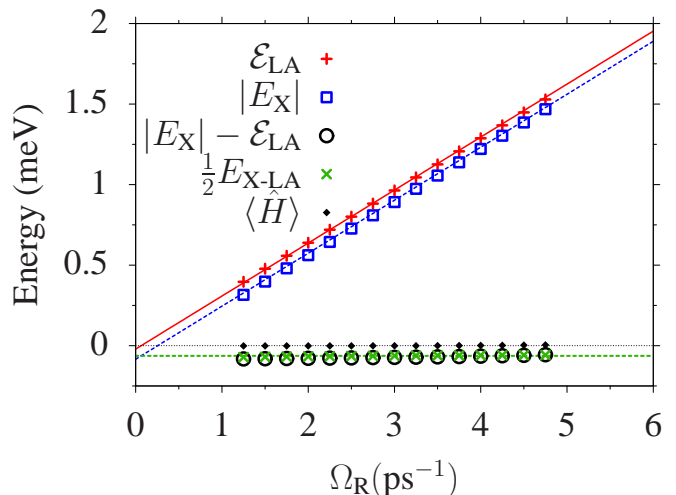


Figure 8: (Color online) Symbols show different energy contributions as labeled in the Figure as a function of the Rabi frequency Ω_R for the case of a cw excitation switched on at $t = 0$. All quantities are calculated at the time $t = 400 \text{ ps}$, i.e., when the QD has reached the steady state. The lines are explained in the text.

the total energy adds up to a larger value. At low Rabi frequencies $\Omega_R \lesssim 1 \text{ ps}^{-1}$ we observe a bright line starting at about 6 ps and a second one starting at about 16 ps indicating that there is essentially no energy transfer at these combinations of time and Rabi frequency. At these low Rabi frequencies the system is close to the adiabatic regime where the polaron is reversibly created and destroyed. Indeed, the bright lines correspond to completed 2π and 4π -rotations and thus to a vanishing exciton occupation, as can be seen by comparison with Fig. 7(a).

As is evident from Fig. 7(a), in a region of Rabi frequencies around the resonant value the exciton occupation reaches its final value of 0.5 within the time window of 20 ps shown in the Figure. Then the whole system, although continuously driven, reaches a steady state and the energy transferred to the phonons saturates. With increasing distance from the resonance condition the steady state is reached at increasingly longer times.

Let us finally investigate quantitatively the energy transfer to the phonon system after the steady state has been reached. For this purpose we have extended the calculations to a time window of 400 ps. During this time for all Rabi frequencies between $\Omega_R \approx 1 \text{ ps}^{-1}$ and $\Omega_R \approx 5 \text{ ps}^{-1}$ the steady state is reached. In Fig. 8 we have plotted the emitted phonon energy \mathcal{E}_{LA} as a function of the Rabi frequency (red crosses). We find that the dependence of the emitted energy on the Rabi frequency is very well described by a linear relationship $\mathcal{E}_{LA} = \frac{1}{2}\hbar\Omega_R - \frac{1}{8}\hbar\omega_{\text{pol}}$ shown as red line.

To understand this behavior let us revisit the model given by Eq. (1) in the case of a driving with a cw light field. It is instructive to rewrite the Hamiltonian in a basis rotating with the light field. This leaves

the phonon part and the exciton-phonon interaction unchanged, while the exciton part including the exciton-light interaction reads

$$\hat{H}_X = \hbar(\omega_x - \omega_L) |x\rangle\langle x| - \frac{\hbar}{2}\Omega_R (|x\rangle\langle g| + |g\rangle\langle x|). \quad (25)$$

In this basis the Hamiltonian is now time-independent thus implying energy conservation, i.e., $\langle \hat{H} \rangle = \text{const.}$ Since before the light field is switched on the QD is in its ground state and no phonons are present, the initial energy is zero. Thus the total energy should remain zero. Introducing the exciton energy

$$E_X = \langle \hat{H}_X \rangle, \quad (26)$$

this leads to

$$\langle \hat{H} \rangle = E_X + E_{LA} + E_{X-LA} = 0. \quad (27)$$

In our simulations we calculate separately all three contributions to the energy. Their sum is plotted by the small black diamonds in Fig. 8 which demonstrates that Eq. (27) is indeed very well satisfied thus confirming the consistency of the correlation expansion approach and the accuracy of the numerics.

In addition to the emitted energy, Fig. 8 shows the absolute value of the exciton energy $|E_X| = -E_X$ (blue squares) and one half of the interaction energy E_{X-LA} (green diagonal crosses). The black circles in Fig. 8 denote the difference between the (negative) exciton energy $|E_X|$ and emitted phonon energy \mathcal{E}_{LA} , which obviously agrees well with one half of the interaction energy. From these results we can conclude that the emitted phonon energy consists of two parts: first the energy $-E_X$ which is released by the relaxation of the exciton and second an energy which is released by the formation of the polaron. Like in the case of pulsed excitation this latter is given by one half of the interaction energy E_{X-LA} . Furthermore we find that the exciton energy is well described by the dependence $|E_X| = \frac{1}{2}\hbar\Omega_R - \frac{1}{2}\hbar\omega_{\text{pol}}$ (blue dashed line) while half of the interaction energy is well represented by $\frac{1}{2}E_{X-LA} = -\frac{3}{8}\hbar\omega_{\text{pol}}$ (green dashed line). However the Figure also indicates that although there is a very good agreement, these dependencies are most probably not exact. In some ranges of Rabi frequencies there are small deviations of the order of at most 10 percent of the polaron energy.

This rises the question whether at least the general behavior of the energies shown in Fig. 8 can be understood from the model. For this purpose the exciton Hamiltonian in the rotating basis given by Eq. (25) is diagonalized leading to the well known dressed states picture. In our case the excitation is in resonance with the polaron shifted exciton transition, thus with respect to the bare exciton energy there is a detuning $\Delta = \omega_L - \omega_x = -\omega_{\text{pol}}$. In the weak coupling limit, i.e., neglecting terms of second order in $\omega_{\text{pol}}/\Omega_R$ the energies of the dressed states read

$$E_{\pm} = \frac{1}{2}\hbar(\omega_{\text{pol}} \pm \Omega_R). \quad (28)$$

Before the light field is switched on the QD is in its ground state $|g\rangle$ with the exciton energy $E_X = 0$. In the dressed state picture this state translates into a superposition between the dressed states $|\psi_{\pm}\rangle$ with the corresponding energies E_{\pm} . In this picture the exciton-phonon interaction is given by

$$\hat{H}_{X-LA} = \sum_{\mathbf{q}} \frac{\hbar}{2} \left(g_{\mathbf{q}} \hat{b}_{\mathbf{q}} + g_{\mathbf{q}}^* \hat{b}_{\mathbf{q}}^{\dagger} \right) \left[|\psi_{+}\rangle\langle\psi_{+}| + |\psi_{-}\rangle\langle\psi_{-}| - |\psi_{+}\rangle\langle\psi_{-}| - |\psi_{-}\rangle\langle\psi_{+}| \right], \quad (29)$$

where again terms of higher order in the polaron energy have been neglected. The interaction now has both diagonal and off-diagonal terms thus leading at low temperatures to a relaxation from the upper to the lower dressed state.^{33,38,51} At sufficiently long times therefore the exciton system ends up in the lower dressed state with the energy $E_X = E_- = \frac{1}{2}\hbar(\omega_{\text{pol}} - \Omega_R)$. Indeed, this agrees with the dashed blue line in Fig. 8 and is thus in excellent agreement with the exciton energies found from the simulations.

The value $E_{X-LA} \approx -\frac{3}{4}\hbar\omega_{\text{pol}}$ cannot so easily be understood. In the case of pulsed excitation we have found $E_{X-LA} = -2f\hbar\omega_{\text{pol}}$ (see Fig. 4), which in the present case would mean $E_{X-LA} = -\hbar\omega_{\text{pol}}$ since the exciton occupation in the lower dressed states is $f = \frac{1}{2}$. On the other hand, the dressed states interaction Hamiltonian in Eq. (29) has in its diagonal a coupling constant of $g_{\mathbf{q}}/2$ which for the lower dressed state should lead to a polaron energy reduced by a factor of 4 and thus to $E_{X-LA} = -\frac{1}{2}\hbar\omega_{\text{pol}}$. The result found from our calculations is in between these two values. This is in line with the results for the long-time exciton state in the presence of a cw field discussed in Ref. 51, where it has been shown that in particular at low temperatures there are slight deviations from both a thermal occupation of the dressed states and from calculations within a weak coupling theory.

Nevertheless it should be pointed out that the discrepancies between the models are in the range of fractions of the polaron energy. Typical Rabi energies are much larger than the polaron energy, thus, as seen in Fig. 8, the total energy transported away from the QD by the LA phonons is in good approximation given by $\mathcal{E}_{LA} = \frac{1}{2}\hbar\Omega_R$.

V. CONCLUSIONS

In conclusion, we have analyzed the spatiotemporal dynamics of the lattice displacement in and around a QD driven by an external electromagnetic field. In general, the displacement field consists of two parts, a localized one which resides in the region of the QD and forms the acoustic polaron and an outgoing strain wave consisting of a single or a series of wave packets. The focus of our investigations has been on the one hand on the energy that is transported by these phonon wave packets and on the other hand on the coherence properties

of the generated phonons. In the case of excitation by Gaussian laser pulses we have found a non-trivial dependence of the emitted acoustic energy on the pulse area and pulse duration. The strongest phonon emission has been found when the time scale of the exciton dynamics, determined by the instantaneous Rabi oscillation period, matches the characteristic phonon time given by the oscillation period of the most strongly coupled phonons. In this case each Rabi cycle of the exciton gives rise to the emission of a pair of phonon wave packets, one with negative and one with positive amplitude. If the exciton dynamics is either much slower or much faster than the phonon dynamics the intensity of the wave packets decreases and, in the limit of very short pulses, the energy may even be further reduced by destructive interference of subsequent wave packets. While for excitation by very short pulses with pulse areas given by odd multiples of π the emitted phonons are almost perfectly coherent, for longer pulses an increasing contribution due to incoherent phonons shows up, as is reflected by the difference between the total and the coherent acoustic Poynting vector.

In the case of continuous excitations switched on instantaneously a series of wave packets with decreasing amplitudes is emitted. The strongest damping is again found for a resonant coupling between exciton and phonon system. Both for much larger and much smaller Rabi frequencies the two systems become increasingly decoupled. While the reduction of the damping of the Rabi oscillations is almost symmetric with respect to the resonant Rabi frequency, the acoustic Poynting vector is much larger for excitation with a Rabi frequency above the phonon resonance because of the larger velocities of the lattice atoms. The energy of the coherent phonons

is emitted as a sequence of pulses with maxima at the edges of the displacement wave packets. In contrast, the total emitted energy is typically a rather smooth function of time given by the envelope over the coherent pulses. Therefore, in a good approximation half of the emitted energy is carried by coherent phonons and the other half by incoherent phonons. The total energy which is transported away from the QD by the phonons increases linearly with the Rabi frequency; it is essentially given by one half of the Rabi energy $\hbar\Omega_R$ which results mainly from the relaxation of the exciton into the lower dressed state but has also a contribution from the polaron dressing process.

Our results thus clearly demonstrate the close connection of the dephasing of the excitonic degrees of freedom with the irreversibility caused by the energy transport away from the QD region by the generated phonons. In addition they shed new light on the coherence properties of these phonons showing that the emitted phonons are in general not completely coherent, but that the coherent phonons carry a rather large part of the total energy (typically about 50 %), which is different from other systems like biased quantum wells, where even under optimal conditions the energy associated with coherent phonons is orders of magnitude smaller than the energy transferred to incoherent phonons.¹¹

Acknowledgments

VMA wishes to thank the Deutsche Forschungsgemeinschaft for financial support within the grant No. AX 17/7-1.

-
- ¹ A. V. Akimov, A. V. Scherbakov, D. R. Yakovlev, C. T. Foxon, and M. Bayer, *Phys. Rev. Lett.* **97**, 037401 (2006).
² A. V. Scherbakov, P. J. S. van Capel, A. V. Akimov, J. I. Dijkhuis, D. R. Yakovlev, T. Berstermann, and M. Bayer, *Phys. Rev. Lett.* **99**, 057402 (2007).
³ J. Huneke, A. Krügel, T. Kuhn, A. Vagov, and V. M. Axt, *Phys. Rev. B* **78**, 085316 (2008).
⁴ H. Gotoh, H. Sanada, H. Yamaguchi, and T. Sogawa, *Appl. Phys. Lett.* **103**, 112104 (2013).
⁵ C. Brüggemann, A. V. Akimov, A. V. Scherbakov, M. Bombeck, C. Schneider, S. Höfling, A. Forchel, D. R. Yakovlev, and M. Bayer, *Nat. Photonics* **6**, 30 (2011).
⁶ R. Blattmann, H. J. Krenner, S. Kohler, and P. Hänggi, *Phys. Rev. A* **89**, 012327 (2014).
⁷ G. C. Cho, W. Kütt, and H. Kurz, *Phys. Rev. Lett.* **65**, 764 (1990).
⁸ R. Merlin, *Solid State Commun.* **102**, 207 (1997).
⁹ O. V. Misochko, *JETP* **92**, 246 (2001).
¹⁰ A. Devos, F. Poinssotte, J. Groenen, O. Dehaese, N. Bertru, and A. Ponchet, *Phys. Rev. Lett.* **98**, 207402 (2007).
¹¹ T. Papenkort, T. Kuhn, and V. M. Axt, *Phys. Rev. B* **81**, 205320 (2010).
¹² X. Hu and F. Nori, *Phys. Rev. Lett.* **76**, 2294 (1996).
¹³ O. V. Misochko, K. Sakai, and S. Nakashima, *Phys. Rev. B* **61**, 11225 (2000).
¹⁴ S. Sauer, J. M. Daniels, D. E. Reiter, T. Kuhn, A. Vagov, and V. M. Axt, *Phys. Rev. Lett.* **105**, 157401 (2010).
¹⁵ A. Hussain and S. R. Andrews, *Phys. Rev. B* **81**, 224304 (2010).
¹⁶ J. Kabuss, A. Carmele, T. Brandes, and A. Knorr, *Phys. Rev. Lett.* **109**, 054301 (2012).
¹⁷ E. M. Gauger and J. Wabnig, *Phys. Rev. B* **82**, 073301 (2010).
¹⁸ I. Wilson-Rae, P. Zoller, and A. Imamoglu, *Phys. Rev. Lett.* **92**, 075507 (2004).
¹⁹ A. Rundquist, A. Majumdar, and J. Vučković, *Appl. Phys. Lett.* **99**, 251907 (2011).
²⁰ I. Yeo, P.-L. de Assis, A. Gloppe, E. Dupont-Ferrier, P. Verlot, N. S. Malik, E. Dupuy, J. Claudon, J.-M. Gérard, A. Auffèves, et al., *Nat. Nanotechnol.* **9**, 106 (2013).
²¹ L. Besombes, K. Kheng, L. Marsal, and H. Mariette, *Phys. Rev. B* **63**, 155307 (2001).
²² B. Krummheuer, V. M. Axt, and T. Kuhn, *Phys. Rev. B* **65**, 195313 (2002).

- ²³ E. Stock, M. R. Dachner, T. Warming, A. Schliwa, A. Lochmann, A. Hoffmann, A. I. Toropov, A. K. Bakarov, I. A. Derebezov, M. Richter, et al., Phys. Rev. B **83**, 041304 (2011).
- ²⁴ P. Borri, W. Langbein, S. Schneider, U. Woggon, R. L. Sellin, D. Ouyang, and D. Bimberg, Phys. Rev. Lett. **87**, 157401 (2001).
- ²⁵ A. Vagov, V. M. Axt, T. Kuhn, W. Langbein, P. Borri, and U. Woggon, Phys. Rev. B **70**, 201305 (2004).
- ²⁶ H. Kamada, H. Gotoh, J. Temmyo, T. Takagahara, and H. Ando, Phys. Rev. Lett. **87**, 246401 (2001).
- ²⁷ A. Zrenner, E. Beham, S. Stufler, F. Findeis, M. Bichler, and G. Abstreiter, Nature (London) **418**, 612 (2002).
- ²⁸ J. Förstner, C. Weber, J. Danckwerts, and A. Knorr, Phys. Rev. Lett. **91**, 127401 (2003).
- ²⁹ P. Machnikowski and L. Jacak, Phys. Rev. B **69**, 193302 (2004).
- ³⁰ P. Borri, W. Langbein, U. Woggon, V. Stavarache, D. Reuter, and A. D. Wieck, Phys. Rev. B **71**, 115328 (2005).
- ³¹ A. Krügel, V. M. Axt, T. Kuhn, P. Machnikowski, and A. Vagov, Appl. Phys. B **81**, 897 (2005).
- ³² A. Vagov, M. D. Croitoru, V. M. Axt, T. Kuhn, and F. M. Peeters, Phys. Rev. Lett. **98**, 227403 (2007).
- ³³ D. P. S. McCutcheon and A. Nazir, New J. Phys **12**, 113042 (2010).
- ³⁴ A. J. Ramsay, A. V. Gopal, E. M. Gauger, A. Nazir, B. W. Lovett, A. M. Fox, and M. S. Skolnick, Phys. Rev. Lett. **104**, 017402 (2010).
- ³⁵ A. J. Ramsay, T. M. Godden, S. J. Boyle, E. M. Gauger, A. Nazir, B. W. Lovett, A. M. Fox, and M. S. Skolnick, Phys. Rev. Lett. **105**, 177402 (2010).
- ³⁶ C. M. Simon, T. Belhadj, B. Chatel, T. Amand, P. Renucci, A. Lemaitre, O. Krebs, P. A. Dalgarno, R. J. Warburton, X. Marie, et al., Phys. Rev. Lett. **106**, 166801 (2011).
- ³⁷ Y. Wu, I. M. Piper, M. Ediger, P. Brereton, E. R. Schmidgall, P. R. Eastham, M. Hugues, M. Hopkinson, and R. T. Phillips, Phys. Rev. Lett. **106**, 067401 (2011).
- ³⁸ S. Lüker, K. Gawarecki, D. E. Reiter, A. Grodecka-Grad, V. M. Axt, P. Machnikowski, and T. Kuhn, Phys. Rev. B **85**, 121302 (2012).
- ³⁹ A. Debnath, C. Meier, B. Chatel, and T. Amand, Phys. Rev. B **86**, 161304 (2012).
- ⁴⁰ P. R. Eastham, A. O. Spracklen, and J. Keeling, Phys. Rev. B **87**, 195306 (2013).
- ⁴¹ D. E. Reiter, D. Wigger, V. M. Axt, and T. Kuhn, Phys. Rev. B **84**, 195327 (2011).
- ⁴² A. Vagov, V. M. Axt, and T. Kuhn, Phys. Rev. B **66**, 165312 (2002).
- ⁴³ D. Wigger, D. E. Reiter, V. M. Axt, and T. Kuhn, Phys. Rev. B **87**, 085301 (2013).
- ⁴⁴ L. Jacak, P. Machnikowski, J. Krasnyj, and P. Zoller, Eur. Phys. J. D **22**, 319 (2003).
- ⁴⁵ B. Krummheuer, V. M. Axt, T. Kuhn, I. D'Amico, and F. Rossi, Phys. Rev. B **71**, 235329 (2005).
- ⁴⁶ P. Machnikowski, V. M. Axt, and T. Kuhn, Phys. Rev. A **75**, 052330 (2007).
- ⁴⁷ V. M. Axt, P. Machnikowski, and T. Kuhn, Phys. Rev. B **71**, 155305 (2005).
- ⁴⁸ B. A. Auld, *Acoustic fields and waves in solids*, vol. 1 (Wiley New York, 1973).
- ⁴⁹ F. Rossi and T. Kuhn, Rev. Mod. Phys. **74**, 895 (2002).
- ⁵⁰ A. Krügel, V. M. Axt, and T. Kuhn, Phys. Rev. B **73**, 035302 (2006).
- ⁵¹ M. Glässl, A. Vagov, S. Lüker, D. E. Reiter, M. D. Croitoru, P. Machnikowski, V. M. Axt, and T. Kuhn, Phys. Rev. B **84**, 195311 (2011).